Journal of Alloys and Compounds 509 (2011) 2663–2666

Contents lists available at ScienceDirect

Journal of Alloys and Compounds

journal homepage: www.elsevier.com/locate/jallcom

Structural, optical and electromagnetic properties of $Bi_{1-x}Ho_xFeO_3$ multiferroic materials

Nguyen Van Minh*, Nguyen Gia Quan

Center for Nano Science and Technology, Hanoi National University of Education, 136 Xuan-Thuy Road, Hanoi, Viet Nam

ARTICLE INFO

Article history:
Received 4 August 2010
Received in revised form 6 December 2010
Accepted 6 December 2010
Available online 13 December 2010

Keywords:
Multiferroics
Raman spectroscopy
Absorption spectra
Impedance
Magnetization

ABSTRACT

$Bi_{1-x}Ho_xFeO_3$ ($x = 0.00$, 0.05, 0.10, 0.15 and 0.20) polycrystalline ceramics were synthesized by a solid-state reaction and their structural, absorption, Raman scattering, impedance and magnetic properties were investigated. The substitution of rare earth Ho for Bi was found to decrease the impurity phase in $BiFeO_3$ ceramics. There appears an anomalous change in the lattice constants, optical band gap as well as the impedance spectroscopy and magnetization of samples at $x = 0.10$, suggesting a limit of dissolubility of Ho doped ions in $BiFeO_3$. Additionally, the Raman measurement performed for the lattice dynamics study of $Bi_{1-x}Ho_xFeO_3$ samples reveals a band centered at around 1000–1300 cm^{-1} which is associated with the resonant enhancement of two-phonon Raman scattering in the multiferroic $Bi_{1-x}Ho_xFeO_3$ samples. Ho-doped $BiFeO_3$ also showed a ferromagnetic-like behavior with $M_r = 1070 \times 10^{-4}$ and $M_s = 1.60$ emu/g for optimum content x = 0.10, which is similar to the solid solution system of $BiFeO_3$.

1. Introduction

Multiferroic materials, which are simultaneously ferroelectric, ferromagnetic and ferroelastic in the same material, have a wide range of potential applications in information storage, spintronic devices and sensors. Among them, the perovskite $BiFeO_3$ is one of the few known magnetoelectric multiferroics, which is ferroelectric ($T_C = 820$–$850\,^\circ C$) [1,2] and antiferromagnetic ($T_N = 370$–$380\,^\circ C$) [1,3]. Recently, partial substitution of Bi^{3+} ions by lanthanides in $BiFeO_3$ has been shown to improve its ferroelectric properties and magnetization [4–7]. Zhang et al. [5] and Das et al. [7] suggested that La^{3+} substitution for Bi^{3+} eliminates impurity phases and destroys the cycloidal spin structure resulting in uniform canted antiferromagnetic ordering. In the studies on dopant effects of Sm [4,8], of Nd [9] in $BiFeO_3$, changes in the crystal structure of the material were observed, which resulted in improved piezoelectric properties, long-range ferroelectric and canted anti-ferromagnetic orders. Uniyal and Yadav [10] claimed on the other hand, that 10 mol% Gd substituted for Bi in the sample compound did not change the crystal structure but only reduced the volume fraction of impurity phases, while decreasing the Neel temperature T_N to ~150 °C from 370 °C, and enhancing the magnetization to the extent of allowing the generation of the ferroelectric hysteresis loops [10]. These phenomena also give rise to unusual dynamical effects, which can be observed in optical experiment which offers the means for elucidating of the driving mechanism of the ferroelectric transition and, eventually, its coupling to magnetic ordering [11,12]. The origins of the ferroelectric order and its coupling to magnetic order are closely related to the lattice dynamics which is in turn directly connected to ferroelectric order. The Raman spectroscopy is known to be a powerful tool for studying the vibrational and magnetic excitations [13]. Some studies on Raman scattering of $BiFeO_3$ have indeed been reported [14], but most of those studies were focused on pure $BiFeO_3$. Although a number of Raman and XRD experiments have also been performed to study the influence of temperature and dopant concentration variations, very little works have been reported on the Ho dopant induced changes in the structure and optical property of $BiFeO_3$. In this paper, we report the result of a study on the Ho doping effects in $Bi_{1-x}Ho_xFeO_3$ by means of measurements and analyses of the XRD pattern as well as the Raman scattering, optical absorption and impedance spectroscopy.

2. Experimental

The $Bi_{1-x}Ho_xFeO_3$ ($x = 0.00$, 0.05, 0.10, 0.15 and 0.20) ceramic samples were prepared by a modified solid-state-reaction method, which adopted a much faster heating and cooling rates in the sintering process than those employed in conventional method. The initial powder material for the synthesis was prepared by mixing appropriate amounts of Bi_2O_3 (Sigma–Aldrich, >99.0%), Ho_2O_3 (Sigma–Aldrich, >99.9%) and Fe_2O_3 (Sigma–Aldrich, 99.9%), which were ground for 4 h in isopropyl alcohol. The powders were thereafter pressed into disks of 10 mm diameter and calcined at 600 °C for 6 h. After calcination the material was ground into a fine powder and leached with 2.5 M nitric acid under continuous stirring for 2 h and washed thoroughly with distilled water. The resulting powder was then dried at 400 °C for 1 h. The powders were then pressed into disks of 10 mm in diameter and 4 mm in thickness, sintered at 825 °C for 10 h with heating rate of 10 °C/min and finally cooled at the rate of 5 °C/min.

* Corresponding author.
E-mail addresses: minhnv@hnue.edu.vn, minhsp@gmail.com (N. Van Minh).

0925-8388/$ – see front matter © 2010 Elsevier B.V. All rights reserved.
doi:10.1016/j.jallcom.2010.12.033

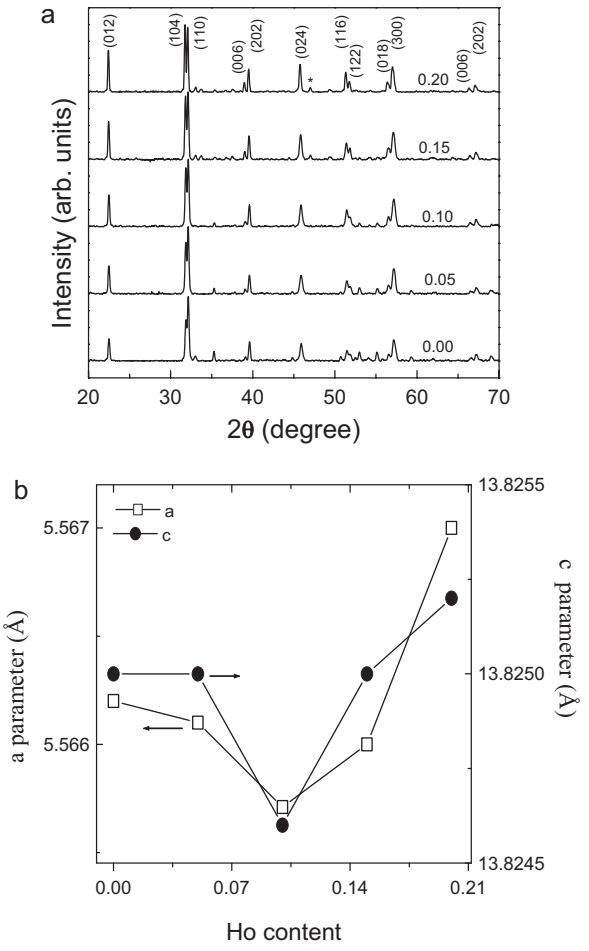

Fig. 1. (a) XRD patterns of $Bi_{1-x}Ho_xFeO_3$ powders and (b) *a*, *c* cell parameters vs. Ho content.

Structural characterization was performed by means of X-ray diffraction using a D5005 diffractometer with Cu Kα radiation and with 2θ varied in the range of 20–70° at a step size of 0.02°. The photoabsorption of $Bi_{1-x}Ho_xFeO_3$ was measured by UV–visible diffuse reflectance spectrometry (Jasco 670 UV–vis spectrometer). Raman measurements were performed in a back scattering geometry using a Jobin Yvon T 64000 triple spectrometer equipped with a cryogenic charge-coupled device (CCD) array detector and operated with 514.5 nm line of Ar ion laser. Impedance spectroscopy was obtained by a Le Croy equipment. The magnetization dependence on magnetic field was measured by a vibrating sample magnetometer (VSM).

3. Result and discussion

Fig. 1a shows the X-ray diffraction patterns of $Bi_{1-x}Ho_xFeO_3$ ($x = 0.00, 0.05, 0.10, 0.15, 0.20$). X-ray diffraction patterns collected for the material obtained after leaching confirmed single phase $BiFeO_3$. Generally, the second phase peaks attributed to Fe or Bi rich phases, $Bi_2Fe_4O_9$ and $Bi_{25}FeO_{40}$ disappeared in these XRD patterns. However, for $x = 0.20$ we observe one foreign peak in the XRD data (asterisk in Fig. 1a). For Ho doped $BiFeO_3$, all peaks are indexed according to the R_{3c} cell of $BiFeO_3$. The lattice parameters deduced for pure $BiFeO_3$ hexagonal unit cell were found to have values $a = 5.577$ Å and $c = 13.868$ Å. These parameters lightly decrease with increasing of Ho content when $x \leq 0.1$. Above this content of Ho, the cell parameters increase. The changes in the cell parameters (Fig. 1b) indicate that the Ho ions have indeed replaced the Bi ions in the unit cell.

The optical property and Raman spectra of pure and doped $BiFeO_3$ were investigated in some published papers [14–17] before. Gao et al. [15] have reported that $BiFeO_3$ nanowires had an energy band gap of about 2.5 eV. According to the UV–visible absorption spectra of $Bi_{1-x}Ho_xFeO_3$ powder (Fig. 2), samples with $x = 0$, 0.05 and 0.1 have an absorption edge, estimated from $(\alpha h\nu)^2$ to $h\nu$ plot [18] is about 2.42 eV, which is consistent with previous report [15,19]. From the inset of Fig. 2 it is clear that the band gaps for samples with $x \leq 0.1$ are very close to each other. This indicates negligible change in electronic structure of BFO with increase in dopant concentration up to $x = 0.1$. However, as we move to higher dopant concentration of $x = 0.15$ and $x = 0.2$, the band gap decreases. This is understood as a consequence of the rearrangements in the molecular orbitals [20]. However, this discussion must be investigated more in details and is in progress.

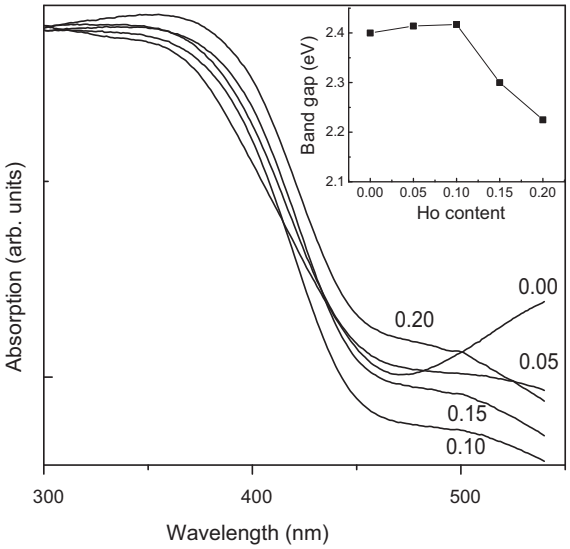

Fig. 2. (a) Absorption spectra of $Bi_{1-x}Ho_xFeO_3$ powders vs. Ho content. The inset shows optical band gap vs. Ho content.

Further effect of Ho substitution is described by the Raman spectra of the $Bi_{1-x}Ho_xFeO_3$ ceramics which are plotted in Fig. 3 with respect to variation of Ho concentration *x* at room temperature. The selection rules for the Raman active modes in rhombohedral $R_{3c}(C_{3v})$ symmetry predict only 13 active Raman phonons with A_1 and E symmetries, according to the rule of decomposition in terms of irreducible representations, $\Gamma_{Raman/IR} = 4A_1 + 9E$. In polarized Raman scattering, the A_1 modes can be observed by parallel polarization, while the E modes can be observed by both parallel and crossed polarizations. Since all these modes fall in the frequency range below ~700 cm^{-1}, most of the Raman studies have been focused in this region, at the cost of missing the information contained at higher frequencies. Here, we measured the Raman spectra in the extended range of 200–1350 cm^{-1}. In addition to the well-understood Raman features in the low frequency region, the spectra show a very prominent band at ~1000–1300 cm^{-1}, which we associate with two-phonon Raman scattering, strongly enhanced due to the resonance with the intrinsic absorption edge.

As seen from Fig. 3a, all samples show the same Raman modes at similar positions. When comparing the low frequency Raman modes (100–700 cm^{-1}) with theoretical and experimental results reported previously [13], a reasonably good agreement is attained. The only difference is the appearance of a prominent additional band around ~1000–1300 cm^{-1} which has rarely been reported before for the doped system. Changing the excitation wavelength to 488 nm led to no observable spectral shifts in this band, thereby confirming its true nature of Raman scattering and, excluding any possible phonon and/or magnon assisted emission in this region. The origin of this spectral band has been assigned to the combination of three different two-phonons Raman scattering in

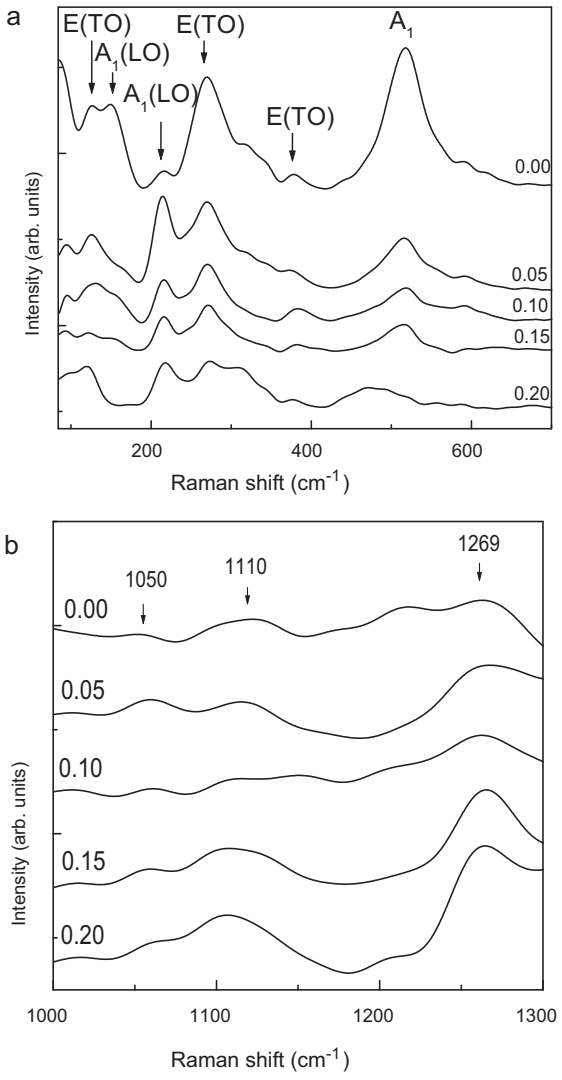

Fig. 3. Raman spectra of $Bi_{1-x}Ho_xFeO_3$ samples ($x = 0.00$, 0.05, 0.10, 0.15 and 0.20).

$BiFeO_3$ [21] labeled as $2A_4$, $2E_8$ and $2E_9$, since their spectral positions practically correspond to twice the energy values of the $A(LO_4) \sim 500\,cm^{-1}$, $E(TO_8) \sim 550\,cm^{-1}$ and $E(TO_9) \sim 620\,cm^{-1}$ normal modes of $BiFeO_3$, respectively. The strong contribution of the two-phonon band to the total Raman spectrum has been attributed to a resonant enhancement with the intrinsic absorption edge in $BiFeO_3$ (2.66 eV) [21,22]. It is seen that larger x generally leads to broader and stronger peaks. The slight difference and inconsistent variation in some of the peaks observed in the investigated samples can be attributed to the different subtle details in the sample preparations. It is known that the synthesis condition sensitively influences the oxygen stoichiometry of the resulted sample. This is expected to lead to changes in oxygen bonding and disorder that are reflected in the frequencies of vibration modes involving oxygen.

The use of impedance spectroscopy to characterize bulk grain, grain boundary and electrode interface contributions by exhibiting successive semicircles (often with some distortion) of the impedance in the complex plane is well established [23]. A high frequency semicircle originates from the bulk conduction and dielectric processes; a low-frequency semicircle is due to ion and electron transfer at the surface contacting the electrode, and an intermediate-frequency semicircle provides information on the grain boundary and/or impurity-phase impedance.

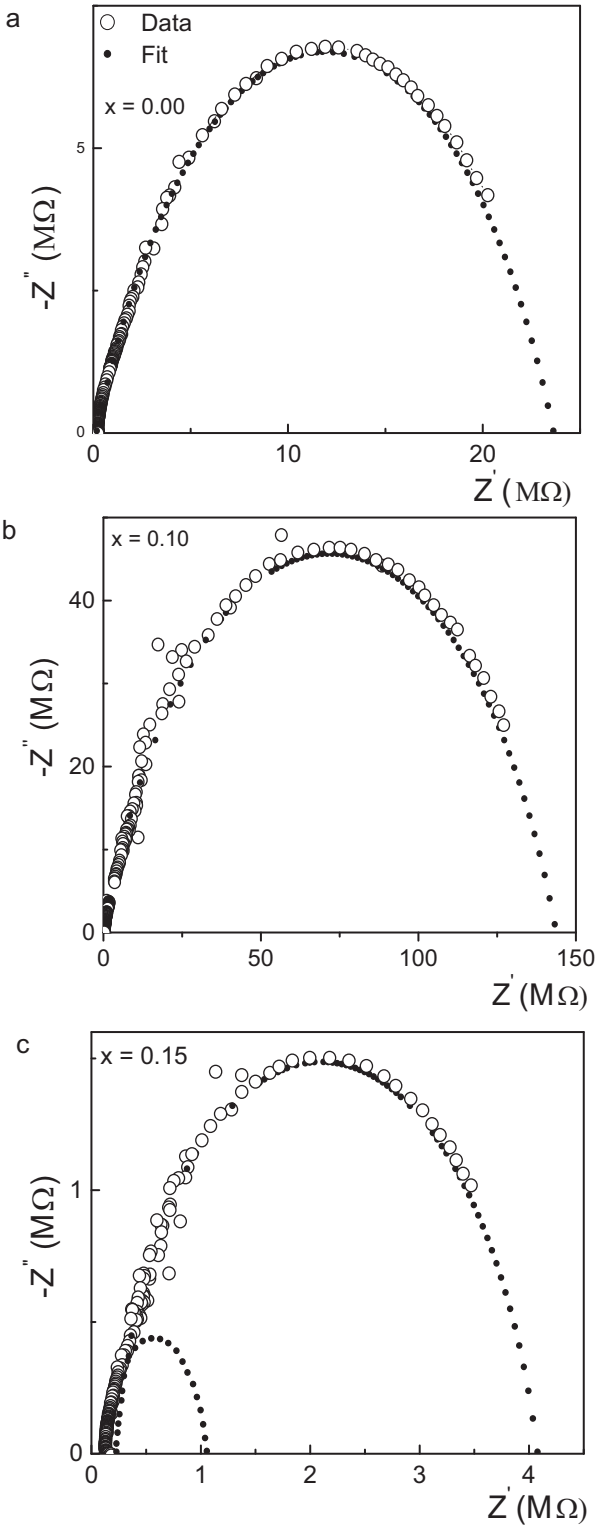

Fig. 4. Impedance spectroscopy of $Bi_{1-x}Ho_xFeO_3$ samples. For clarity, we show spectroscopy for (a) $x = 0.00$, (b) $x = 0.10$, and (c) $x = 0.15$.

Fig. 4 presents the impedance spectroscopy of the $Bi_{1-x}Ho_xFeO_3$ samples. The impedance spectroscopy of samples of $x = 0.00$, $x = 0.05$ and $x = 0.10$ is almost similar to each other; the same way for samples with $x = 0.15$ and $x = 0.20$. Therefore, we show only the spectroscopy of samples with $x = 0.00$, 0.10 and 0.15, for clarity. From these results we can identify the difference in grain and grain boundary properties vs. Ho doping content.

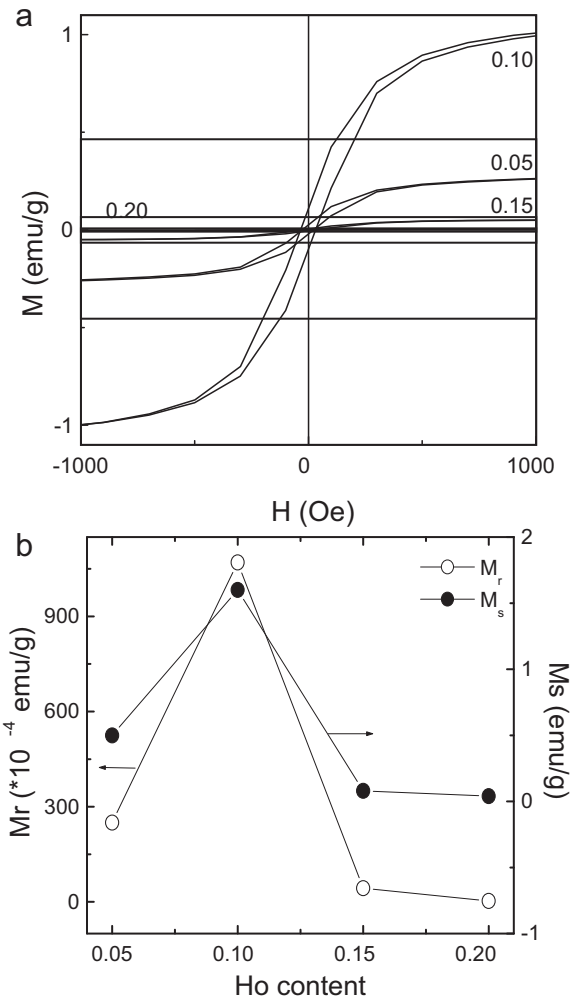

Fig. 5. (a): Magnetization vs. magnetic field of $Bi_{1-x}Ho_xFeO_3$ powders and (b) M_r and M_s vs. Ho content.

Fig. 4a and b shows the Cole–Cole plot of samples with $x = 0.00$ and $x = 0.10$. The spectrum of the sample with $x = 0.15$ (Fig. 4c) shows two separated semicircles and it is clear that the impedance does not tend towards the zero in the complex plane. The semicircles attributed to the grain boundaries and electrodes are relatively large and the high-frequency semicircle seems to have disappeared. The sample with a relatively high Ho content might lead to high grain boundary resistivity. However, below $x = 0.10$, the contribution of grain to the impedance still dominates (Fig. 4a and b).

The magnetization–magnetic field (M–H) curves of $Bi_{1-x}Ho_xFeO_3$ ceramics were measured with a maximum magnetic field of 15 kOe, as shown in Fig. 5a. In fact, $BiFeO_3$ is known to be antiferromagnetic having a G-type magnetic structure [24], but has a residual magnetic moment due to a canted spin structure (weak ferromagnetic) [3]. However, the Ho-doped specimens exhibited a magnetic hysteresis loop, referring to a ferromagnetic behavior. As shown in Fig. 5a, the curves of $x \geq 0.05$ are clearly not collinear. The saturation magnetization (M_s) are 0.50, 1.60, 0.075 and 0.04 emu/g for $x = 0.05$, 0.10, 0.15 and 0.20, respectively. The remnant magnetizations (M_r) are 250×10^{-4}, 1070×10^{-4}, 43×10^{-4} and 3×10^{-4} emu/g, respectively. The M_s and M_r values as the function of x are plotted in the Fig. 5b. A relevant research [25] reported that the Y substitution could suppress the spin cycloid of $BiYFeO_3$. Further analysis reveal that the M_s and M_r values of $Bi_{1-x}Ho_xFeO_3$ with $x = 0.15$ and 0.20 are significantly bigger than those of others, suggesting that with $x < 0.10$, the Ho-substitution can only suppress but cannot destruct the spin cycloid, which is responsible for the limited and smooth increase of the M_s and M_r values. However, when $x \geq 0.10$, the Ho-substitution result in a structural phase transition wherein the spin cycloid may be destructed, so that the latent magnetization locked within the cycloid may be released, and a significant increased M_s and M_r values is observed. However, when $x \geq 0.10$, another phase can be formed, which also can contribute to the increase of magnetization value. Whether Ho-substitution can improve the saturation magnetization so much should be discussed more and another effective analytical method should be introduced to clarify the issue.

4. Conclusion

In summary, the dopant induced changes in the structure, optical absorption, Raman scattering spectra, impedance and magnetization of $Bi_{1-x}Ho_xFeO_3$ samples have been investigated. It is shown that $Bi_{1-x}Ho_xFeO_3$ crystallizes in the rhombohedral crystal structure at room temperature with the space group R_{3c}. The cell parameters, optical band gaps, impedance and magnetization of $Bi_{1-x}Ho_xFeO_3$ samples exhibit the abrupt change at x around 0.10, suggesting the limit of dissolubility of Ho doped ions in $BiFeO_3$. The Raman scattering measurement reveals a prominent two-phonon band around 1000–1150 cm^{-1}. The Ho dopant in the limit of dissolubility has improved the magnetization of $BiFeO_3$ compound.

Acknowledgment

This work has been supported by Vietnam's National Foundation for Science and Technology Development (NAFOSTED) of Vietnam.

References

[1] Y.E. Roginskaya, et al., Sov. Phys. JETP 23 (1966) 47.
[2] F. Kubel, H. Schmid, Acta Cryst. B 46 (1990) 698.
[3] S.V. Kiselev, R.P. Ozerov, G.S. Zhdanov, Sov. Phys. Dokl. 7 (1963) 742.
[4] K.S. Nalwa, A. Grag, A. Upadhyaya, Mater. Lett. 62 (2008) 878.
[5] S.T. Zhang, et al., Appl. Phys. Lett. 88 (2006) 162901.
[6] Y.H. Lee, J.M. Wu, C.H. Lai, Appl. Phys. Lett. 88 (4) (2006) 042903.
[7] S.R. Das, et al., J. Appl. Phys. 101 (2007) 034104.
[8] G.L. Yuan, S.W. Or, J. Appl. Phys. 100 (2006) 024109.
[9] G.L. Yuan, S.W. Or, Appl. Phys. Lett. 89 (2006) 052905.
[10] P. Uniyal, K.L. Yadav, Mater. Lett. 62 (2008) 2858.
[11] A.B. Souchkov, et al., Phys. Rev. Lett. 91 (2003) 027203.
[12] A.P. Litvinchuk, et al., J. Phys.: Condens. Matter 16 (2004) 809.
[13] M. Cazayous, et al., Phys. Rev. Lett. 101 (2008) 037601, and references therein.
[14] Y. Yang, J.Y. Sun, K. Zhu, Y.L. Liu, J. Chen, X.R. Xing, Physica B 404 (2009) 171.
[15] F. Gao, et al., Appl. Phys. Lett. 89 (2006) 102506.
[16] X.S. Xu, et al., Phys. Rev. B 79 (2009) 134425.
[17] Xiong Wang, Yan'ge Zhang, Zhibin Wu, Mater. Lett. 64 (2010) 486.
[18] M.A. Butler, J. Appl. Phys. 48 (1977) 1914.
[19] H. Katsura, A.V. Balatsky, N. Nagaosa, Phys. Rev. Lett. 98 (2007) 027203.
[20] B. Bhushan, et al., Solid State Sci. 12 (2010) 1063.
[21] O. Mariola, Ramirez, et al., Appl. Phys. Lett. 92 (2008) 022511.
[22] S.R. Basu, et al., Appl. Phys. Lett. 92 (2008) 091905.
[23] J.R. Macdonald, Impedance Spectroscopy, Willey, New York, 1987.
[24] A.J. Jacobson, B.E.F. Fender, J. Phys. C: Solid State Phys. 8 (1975) 844.
[25] R.K. Mishra, et al., J. Phys.: Condens. Matter 20 (2008) 045218.